

Synthesis, Characterization, and Relative Stabilities of Self-Assembled Monolayers on Gold Generated from Bidentate *n*-Alkyl Xanthic Acids

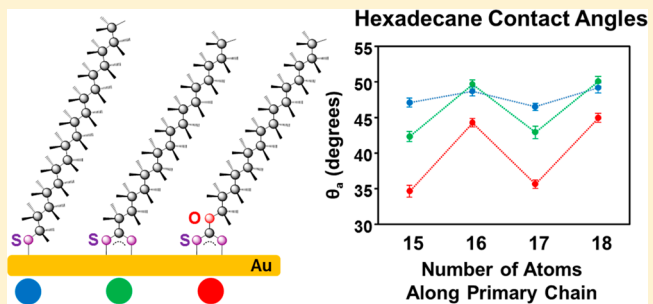
H. Justin Moore,*† Ramon Colorado, Jr.,† Han Ju Lee,† Andrew C. Jamison,† and T. Randall Lee*,†

*Department of Chemistry and Environmental Sciences, University of Texas at Brownsville, Brownsville, Texas 78520, United States

†Department of Chemistry and the Texas Center for Superconductivity, University of Houston, Houston, Texas 77204-5003, United States

S Supporting Information

ABSTRACT: A series of self-assembled monolayers (SAMs) on gold were generated by the adsorption of *n*-alkyl xanthic acids (NAXAs) having the general formula $\text{CH}_3(\text{CH}_2)_n\text{OCS}_2\text{H}$ ($n = 12–15$). The structural features of these SAMs were characterized by optical ellipsometry, contact angle goniometry, polarization modulation infrared reflection absorption spectroscopy (PM-IRRAS), and X-ray photoelectron spectroscopy (XPS). This series of xanthate SAMs were compared to SAMs generated from the corresponding *n*-alkanethiols and aliphatic dithiocarboxylic acids (ADTCAs). The collected data indicate that the NAXAs generate densely packed and well-ordered monolayers. The contact angles of hexadecane on the xanthate monolayers exhibited a large “odd–even” effect similar to that produced by the ADTCA SAMs. The relative stability of these bidentate xanthate SAMs was evaluated by monitoring the changes in ellipsometric thicknesses and wettability as a function of time under various conditions. The results demonstrate that SAMs formed from NAXAs are much less stable than analogous *n*-alkanethiolate and ADTCA SAMs.



INTRODUCTION

Self-assembled monolayers (SAMs) of *n*-alkanethiols on Au(111) are one of the most studied organosulfur-based thin films because they form well-ordered, highly oriented assemblies when adsorbed from solution.^{1–4} The molecular architecture of an alkanethiolate adsorbate on gold can be divided into three parts: the thiolate headgroup that binds strongly to the substrate, the tailgroup that comprises the exposed chemical functionality of the SAM interface, and the hydrocarbon spacer that stabilizes the aligned assembly through van der Waals forces, providing a link between the headgroup and the tailgroup. Interest in alkanethiol-based SAMs also derives from their versatility, stemming from the ability to modify systematically any section of their architecture through chemical synthesis. Such flexibility in the design of organosulfur adsorbates enables the preparation of tailored surfaces to elicit specific interfacial or structural properties. Additionally, the length of the hydrocarbon spacer can be adjusted to generate surfaces of precise thicknesses. As a result, an overwhelming array of alkanethiol-based SAMs on gold have been explored as two-dimensional model surfaces to explore fundamental structure–property relationships and interfacial phenomena such as wetting, adhesion, and friction.

The interfacial properties of SAMs also depend on film organization and structure. The orientation and packing of alkanethiolate adsorbates on gold vary with the headgroup

spacing and van der Waals interactions between neighboring adsorbates.^{2,5–7} Further investigations have focused on integrating diverse sulfur-containing headgroups such as bidentate^{8–14} and tridentate^{8,15–19} thiols, dithiocarboxylic acids,^{20–22} dialkyldithiocarbamates,^{23–25} and dialkyldithiophosphinic acids,^{26–28} in hopes of preparing surfaces having unique interfacial, chemical, and structural properties by inducing unconventional adsorbate geometries and surface binding properties. Of particular relevance, Lee and co-workers investigated a variety of SAMs generated from bidentate aliphatic dithiocarboxylic acids (ADTCAs).^{20–22}

While *n*-alkanethiolates on Au(111) have been reported to produce an array that is commensurate with the occupation of 3-fold hollow sites on gold where neighboring sulfur atoms reside $\sim 5.0 \text{ \AA}$ apart (next-nearest-neighbor bonding site spacing),^{29–31} the distance between the centers of the two sulfur atoms in ADTCAs is $\sim 2.87 \text{ \AA}$.²⁰ Since the nearest-neighbor spacing on Au(111) is $2.9 \pm 0.3 \text{ \AA}$,³² ADTCAs presumably occupy sites on the gold lattice upon the formation of SAMs that produce a substantially different surface arrangement than what occurs with *n*-alkanethiolate SAMs. This assumption is supported by the observations of Li et al. in

Received: March 29, 2013

Revised: July 19, 2013

Published: July 22, 2013



an STM study of the surface structures of octanethiolate SAMs on gold.³³ These authors claim a shift in neighboring adsorbates to adjacent fcc and hcp hollow sites helps explain the occurrence of one form of the $c(4 \times 2)$ lattice structure found in SAMs on Au(111). Additionally, Colorado and co-workers used XPS to show that the adsorbates in a well-organized ADTCA SAM bond to the surface of gold through both sulfur atoms.²⁰

Although *n*-alkanethiol and ADTCA adsorbates possess identical backbone structures, the bidentate $-CS_2$ headgroup of the ADTCA SAMs apparently gives rise to alkyl chain conformations that are unlike those of *n*-alkanethiolate SAMs. Contact angle measurements and surface IR spectroscopy confirmed the structural differences between these two types of SAMs. Advancing hexadecane contact angle (θ_a^{HD}) measurements on the ADTCA SAMs showed extraordinarily large “odd–even” effects: contact angles are higher on films composed of even-numbered hydrocarbon chain lengths and lower on films composed of odd-numbered hydrocarbon chain lengths. This odd–even effect has been observed in numerous other examinations of *n*-alkanethiolate SAMs³⁴ and is frequently attributed to terminal group orientations, reflecting either a greater wettability of methylene vs methyl groups³⁵ or the increased density of atomic contacts made between the SAM interface and the contacting liquid.³⁶ To confirm that the wettability differences could be attributed to terminal group orientation, polarization modulation infrared reflection absorption spectroscopy (PM-IRRAS) was employed to characterize the surface structure of the ADTCA SAMs.^{20,21} Evaluation of the surface IR spectra revealed that the net dipole associated with the symmetric vibrations of the C–H bonds for the terminal methyl groups ($\nu_s^{CH_3}$) of the ADTCA SAMs composed of even-numbered hydrocarbon chains was oriented approximately perpendicular to the surface; however, with the ADTCA SAMs composed of odd-numbered hydrocarbon chains, $\nu_s^{CH_3}$ was oriented more parallel to the surface than analogous *n*-alkanethiolate SAMs. In fact, a recent study by Cimatu et al. using sum frequency generation imaging microscopy (SFGIM) found that the difference in micro-contact-printed monolayers of ADTCA SAMs having either even or odd numbers of hydrocarbon chain lengths could be used to enhance the image contrast in patterned surfaces based solely on the change in orientation of the terminal methyl groups.³⁷

In an effort to further our understanding of the structural relationships of monolayers having divergent molecular headgroups, we chose to evaluate the structural and interfacial properties of SAMs of *n*-alkyl xanthic acids (NAXAs) on gold. Alkyl xanthates have been proposed as useful tools in colloid science because they possess unique properties derived from their relative instability as compared to alkanethiols.³⁸ This aspect of these potential SAM headgroups might facilitate their use as temporary or thermally decomposable capping and protecting agents of small metal colloids.^{39,40} Additionally, prior research on ADTCA SAMs has demonstrated the potential for adsorbates that form well-ordered films but are subject to easy removal, rendering them suitable as transient protecting agents in soft lithographic patterning.²² Additional background regarding the role of adsorbate stability in SAM research can be found in recent reviews by Chinwangso et al. and Srisombat et al.^{41,42}

In the investigation described in this report, we explore the structure, interfacial properties, and relative stability of

bidentate SAMs generated from NAXAs of the form $CH_3(CH_2)_nOCS_2H$ where $n = 12–15$, as shown in Figure 1.

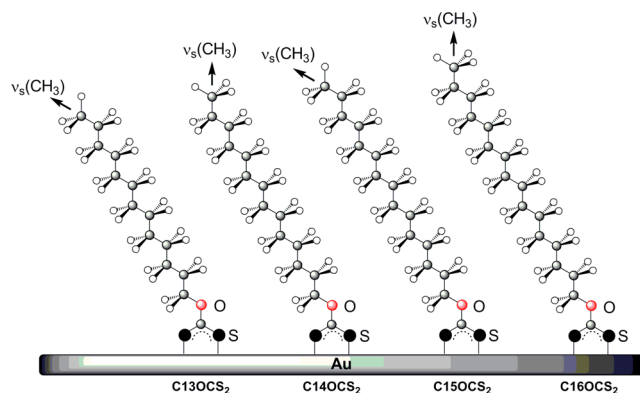


Figure 1. Illustration of the structures of *n*-alkyl xanthates on gold depicting the terminal methyl group orientation of adsorbates possessing odd and even numbers of atoms along the backbone of their primary chains.

We compare this new series of monolayers to those generated from their *n*-alkanethiol analogues, $CH_3(CH_2)_nSH$ where $n = 14–17$, and from comparable ADTCAs, $CH_3(CH_2)_nCS_2H$ where $n = 13–16$. Prior reports investigating the adsorption of *n*-alkyl xanthic acids or *n*-alkyl xanthates on gold are few and generally involve ethyl xanthate monolayers, films that provide little insight regarding the ordering of alkyl chains bearing these headgroups.^{43–46} At the beginning of this project, we anticipated that *n*-alkyl xanthate SAMs would exhibit similar “odd–even” effects to SAMs formed from ADTCAs, as revealed by their wettability data and determined by the number of atoms forming their primary chain (carbon and oxygen atoms). Additionally, we wished to determine if the influences that created such unusual wettability data would provide unique trends within other data sets collected for these SAMs. And, since a prior study investigating ADTCA SAMs by Lee et al.²¹ produced data that showed reduced stabilities under ambient conditions for such SAMs, we compared the stability of SAMs formed from *n*-alkanethiols, ADTCAs, and NAXAs under various conditions to determine their relative stabilities.

EXPERIMENTAL SECTION

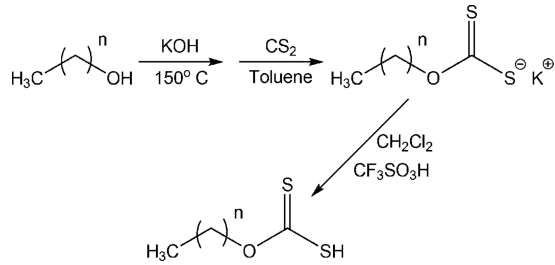
Materials. Gold shot (99.99%) was purchased from Americana Precious Metals. Chromium rods (99.9%) were purchased from R.D. Mathis Company. Single-crystal silicon (100) wafers, which were polished on one side, were acquired from North East Silicon Technologies and rinsed with absolute ethanol (Aaper Alcohol and Chemical Co.) before use. The liquids used for contact angle measurements were of the highest purity available from Aldrich Chemical Co. and were used as received from the supplier. *n*-Alkanethiols used to generate SAMs were either commercially available or synthesized using established methods.

Toluene and methylene chloride (EM Science) were dried by passing through an alumina-packed column. The normal alkyl alcohols used in the synthesis of the *n*-alkyl xanthates were commercially available (Aldrich Chemical Co.) and used as received. Carbon disulfide (CS_2) and trifluoromethanesulfonic acid were purchased from Aldrich Chemical Co. and were of the highest purity available. Potassium hydroxide and acetone (EM Science) were used as received. Diethyl ether (EM Science) was distilled from calcium hydride (CaH_2 ; Aldrich Chemical Co.) to remove water and the stabilizer butylated hydroxytoluene (BHT). Nuclear magnetic resonance (NMR) spectra were recorded on a JEOL ECA-500 spectrometer operating at 500

MHz for ^1H NMR and 125 MHz for ^{13}C NMR. The spectra were obtained in chloroform-*d* purchased from Cambridge Isotope Laboratories, and chemical shifts were referenced to δ 7.26 for ^1H and δ 77.11 for ^{13}C spectra.

The series of alkyl xanthic acids (abbreviated CxOCS_2H , where $x = 13–16$) were synthesized from the corresponding alkyl alcohols via alkoxide addition to CS_2 according to a published procedure.⁴⁷ The synthesis strategy is shown in Scheme 1 and was used to prepare all

Scheme 1. Synthesis of *n*-Alkyl Xanthic Acids



four alkyl xanthic acids in this study. These acids were then converted to alkyl xanthates and stored as their potassium salts due to the fragile nature of the free acids. Subsequently, each compound was converted to the acid form when needed for the preparation of SAM solutions and NMR characterization (see below and the Supporting Information).

***n*-Hexadecyl Xanthic Acid ($\text{C16OCS}_2\text{H}$).** *n*-Hexadecyl potassium xanthate was prepared by heating 3.0 g (13 mmol) of hexadecanol to 150 °C with 0.70 g (13 mmol) of KOH. To this was added, with stirring, 100 mL of toluene held at 100 °C, to which 0.95 g (13 mmol) carbon disulfide was added dropwise at room temperature with vigorous stirring. The thick suspension that formed was stirred for 1 h and diluted with 100 mL of diethyl ether and then stirred for an additional 2 h. The product was filtered on a sintered glass funnel, washed with diethyl ether, and dried. The product was purified by washing with 20 mL of cold water, followed by vacuum-drying, recrystallizing from acetone, and then washing again with diethyl ether. Hexadecyl potassium xanthate was obtained in 62% yield. Hexadecyl xanthic acid was prepared by placing 0.050 g (0.14 mmol) of hexadecyl potassium xanthate in a sealed and purged 50 mL round-bottomed flask with a small stir bar and 25 mL of dry CH_2Cl_2 . To this suspension was added 1.4 mL of 0.1 M trifluoromethanesulfonic acid in dry CH_2Cl_2 , which was stirred vigorously for 20 min. The resulting solution was filtered to remove any inorganic salts through a 0.22 μm syringe filter and dried over MgSO_4 , and the solvent was removed by rotary evaporation to afford *n*-hexadecyl xanthic acid, $\text{CH}_3(\text{CH}_2)_{15}\text{OCS}_2\text{H}$. ^1H NMR (500 MHz, CDCl_3): δ 5.55 (bs, 1H), 4.48 (t, $J = 6.9$ Hz, 2 H), 1.74–1.80 (m, 2 H), 1.25–1.40 (m, 24 H), 0.87 (t, $J = 6.9$ Hz, 3 H). ^{13}C NMR (125 MHz, CDCl_3): δ 209.41, 75.01, 32.02, 29.75, 29.64, 29.56, 29.46, 29.27, 28.18, 25.89, 22.79, 14.24.

***n*-Pentadecyl Xanthic Acid ($\text{C15OCS}_2\text{H}$).** ^1H NMR (500 MHz, CDCl_3): δ 5.54 (bs, 1H), 4.48 (t, $J = 6.9$ Hz, 2 H), 1.74–1.80 (m, 2 H), 1.25–1.40 (m, 24 H), 0.87 (t, $J = 6.9$ Hz, 3 H). ^{13}C NMR (125 MHz, CDCl_3): δ 209.41, 75.02, 32.02, 29.75, 29.63, 29.56, 29.46, 29.27, 28.18, 25.89, 22.79, 14.23.

***n*-Tetradecyl Xanthic Acid ($\text{C14OCS}_2\text{H}$).** ^1H NMR (500 MHz, CDCl_3): δ 5.54 (bs, 1H), 4.48 (t, $J = 6.9$ Hz, 2 H), 1.74–1.80 (m, 2 H), 1.25–1.40 (m, 22 H), 0.87 (t, $J = 6.9$ Hz, 3 H). ^{13}C NMR (125 MHz, CDCl_3): δ 209.41, 75.02, 32.02, 29.75, 29.63, 29.56, 29.46, 29.28, 28.18, 25.89, 22.79, 14.23.

***n*-Tridecyl Xanthic Acid ($\text{C13OCS}_2\text{H}$).** ^1H NMR (500 MHz, CDCl_3): δ 5.54 (bs, 1H), 4.47 (t, $J = 6.9$ Hz, 2 H), 1.74–1.79 (m, 2 H), 1.25–1.41 (m, 20 H), 0.87 (t, $J = 6.9$ Hz, 3 H). ^{13}C NMR (125 MHz, CDCl_3): δ 209.41, 75.02, 32.02, 29.73, 29.63, 29.56, 29.45, 29.27, 28.18, 25.88, 22.79, 14.23.

Preparation of SAMs. Solutions of the xanthic acids, dithiocarboxylic acids, and *n*-alkanethiols were prepared in weighing bottles

previously cleaned in piranha solution (7:3 H_2SO_4 /30% H_2O_2) for 1 h. *Caution: piranha solution reacts violently with organic materials and should be handled with appropriate care.* The weighing bottles were then rinsed with deionized water and absolute ethanol. The gold substrates were prepared by thermal evaporation/vapor deposition of ~ 100 Å of chromium as an adhesion promoter on the polished surfaces of the silicon wafers, followed by deposition of ~ 1000 Å of gold. The vacuum pressure in the chamber was maintained at $\sim 2 \times 10^{-5}$ Torr during the deposition of both chromium and gold. The freshly prepared gold-coated wafers were immediately cut into slides ($\sim 1 \times 3$ cm) with a diamond-tipped stylus. The slides were then rinsed with absolute ethanol and dried with a stream of ultrapure nitrogen gas. The optical constants for the bare gold substrates were collected, the slides were then rinsed with ethanol, and the slides were immersed in the adsorbate solutions: xanthic acids (1 mM in methylene chloride), dithiocarboxylic acids (1 mM in ethanol), and *n*-alkanethiols (1 mM in ethanol). All xanthic acid and ADTCA solutions were prepared immediately following purification of the acids; only freshly prepared developing solutions were used for the formation of SAMs. All developing SAMs were allowed to equilibrate for a period of 48 h. The resulting xanthic acid SAMs were rinsed with ethanol, methylene chloride, toluene, and dried with ultrapure nitrogen gas before immediate characterization. The ADTCA and *n*-alkanethiol SAMs were thoroughly rinsed with ethanol and dried with ultrapure nitrogen gas before immediate characterization.

Ellipsometric Thicknesses. Thicknesses were measured using a Rudolph Research Auto EL III ellipsometer, which consists of a He-Ne laser (632.8 nm) at an incident angle of 70°. The refractive index was assumed to be 1.45 for all films, in accord with prior work.^{20,21,41} For each sample, the calculated value represents an average of measurements taken on three separate slides, with data collected for three spots per slide.

Contact Angle Wettabilities. Advancing contact angles (θ_a) were measured using a ramé-hart model 100 contact angle goniometer. The contacting liquids, hexadecane ($\text{C}_{16}\text{H}_{34}$, HD) and water (H_2O , W), were dispensed and withdrawn utilizing a Matrix Technologies micro-Electrapipet 25 operated at 1 $\mu\text{L}/\text{s}$. For each sample, the calculated value represents an average for measurements taken on three separate slides, with data collected for three spots per slide and measurements recorded for both drop edges for each drop. The measurements were performed at 293 K with the pipet tip remaining in contact with the drop throughout the procedure.

Infrared Spectroscopy. A Nicolet MAGNA-IR 860 Fourier transform spectrometer having a liquid-nitrogen-cooled mercury–cadmium–telluride (MCT) detector and a Hinds Instruments PEM-90 photoelastic modulator was used to collect the PM-IRRAS data. The IR beam was reflected off the sample at an incident angle of 80°. Each spectrum consisted of 512 scans collected at a spectral resolution of 4 cm^{-1} .

X-ray Photoelectron Spectroscopy. A PHI 5700 XPS having a monochromatic Al $K\alpha$ X-ray source ($h\nu = 1486.7$ eV) and a beam incident at 90° relative to the axis of a hemispherical energy analyzer was used to obtain XPS spectra from freshly prepared samples. The spectrometer was configured to operate at high resolution with a pass energy of 23.5 eV, a photoelectron takeoff angle of 45° from the surface, and an analyzer spot diameter of 2 mm. Spectra were collected at room temperature at a base pressure of 2×10^{-9} Torr. For every ten scans accumulated to obtain the C_{1s} and O_{1s} spectra, 5 and 25 scans were accumulated to obtain the Au_{4f} and S_{2p} spectra, respectively, all over a 20 min time frame.

RESULTS AND DISCUSSION

Thicknesses of the Films. Ellipsometry is commonly used to determine the thickness of organic thin films.⁷ Although experimental uncertainties (e.g., a typical standard deviation within ± 2 Å) exist when using ellipsometry in thin-film characterizations,^{48–50} this technique has proven reliable for verifying thickness changes in a series of films that systematically differ in structure by only a few carbons atoms.⁴⁸ We

compared the average ellipsometric thicknesses of SAMs generated from the *n*-alkyl xanthates to the thicknesses of SAMs generated from their ADTCA and *n*-alkanethiol analogues. Figure 2 shows that the plotted thickness data of

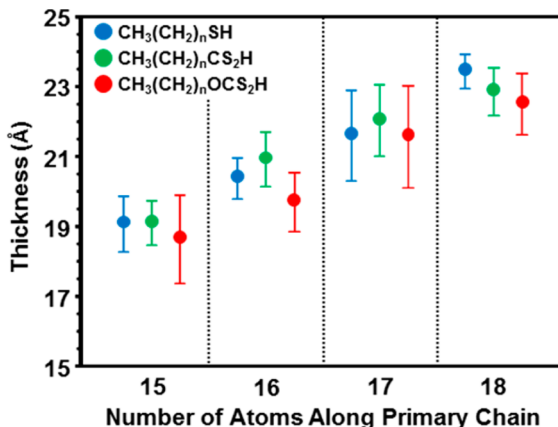


Figure 2. Ellipsometric thicknesses of SAMs generated from *n*-alkanethiols, dithiocarboxylic acids, and *n*-alkyl xanthic acids. The *x*-axis represents the total number of atoms in the chain's backbone, a number that is not necessarily equal to *n*. The symbols in this figure are offset to avoid overlap of the error bars. Error bars indicate the standard deviation for the data.

the ADTCA and *n*-alkanethiol SAMs are nearly indistinguishable. As a whole, these data suggest that the NAXAs generate films of monomolecular thickness, producing an array of alkyl chains extending away from the surface in a densely packed arrangement. However, the thicknesses of the SAMs generated from all four NAXA adsorbates are slightly less than those of the other SAMs (by ≤ 1 Å). The slightly diminished thicknesses, which are within experimental error, might be an indication of some disorder in the film or an increase in the average chain tilt when compared to *n*-alkanethiolate SAMs on gold ($\sim 30^\circ$ from the surface normal).⁸ A change in chain tilt might arise from structural changes associated with the introduction of an oxygen atom in place of a methylene unit near the headgroup. Such a structural change close to the headgroup in the NAXA adsorbates can plausibly lead to at least two changes in the SAM structure. First, C–O bond lengths are shorter (~ 1.4 Å) than C–C bond lengths (~ 1.5 Å), which can account for a small portion of the observed diminished ellipsometric thicknesses in the NAXA SAMs.⁵¹ Second, a greater tilting of the alkyl chains from the surface normal might arise from the presence of the nonbonding lone pair electrons on the oxygen atom, reducing the C–O–C bond angle (as compared to a C–C–C bond angle), thus decreasing the observed ellipsometric thicknesses in NAXA SAMs (see Figure 1). Notably, this latter effect would only provide a minimal reduction in thickness, if any.⁵¹

Wettabilities. Contact angle measurements are known to be sensitive to the conformational order and interfacial structure of organic thin films.⁷ The wettabilities of SAMs generated from the NAXAs were compared to the corresponding SAMs generated from ADTCAs and *n*-alkanethiols. As can be seen in Figure 3, the average advancing contact angle of water ($\theta_a^{\text{H}_2\text{O}}$) for all the SAMs in all three series is within $\pm 2^\circ$ of 115° . These data suggest that films formed from these three types of SAMs are similarly hydrophobic, consistent with SAMs terminated by methyl groups. Additionally, the data indicate

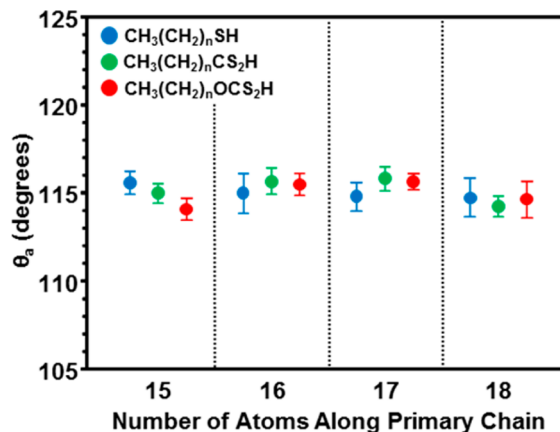


Figure 3. Advancing contact angles of water on SAMs generated from *n*-alkanethiols, dithiocarboxylic acids, and *n*-alkyl xanthic acids. The *x*-axis represents the total number of atoms in the chain's backbone, a number that is not necessarily equal to *n*. The symbols in this figure are offset to avoid overlap of the error bars. Error bars indicate the standard deviation for the data.

that all three types of films present interfaces of sufficient order and organization that they produce data that are statistically equivalent. In contrast, Park et al. found that SAMs formed from a series of bidentate adsorbates having a different headgroup but an exposed interface of alkyl chains similar in length to those examined here gave $\theta_a^{\text{H}_2\text{O}}$ values that were ~ 5 – 8° lower than those of SAMs formed from *n*-alkanethiols.⁸

Dispersive liquids such as hexadecane (HD) are often used to probe low-energy surfaces because they are particularly sensitive to the composition and interfacial structure of hydrocarbon-based SAMs.⁵² For the present study, the advancing contact angles of hexadecane (θ_a^{HD}) were collected on the three series of SAMs to probe the dispersive interfacial energy of these films. As can be seen in Figure 4, all three types of SAMs exhibit a similar zigzag pattern where the contact angles are lower on SAMs having an odd-numbered chain length. This type of odd–even effect has been attributed to the greater accessibility of the more wettable methylene units by solvent molecules on odd-numbered chain length SAMs since the terminal C–C bond is tilted further from the surface

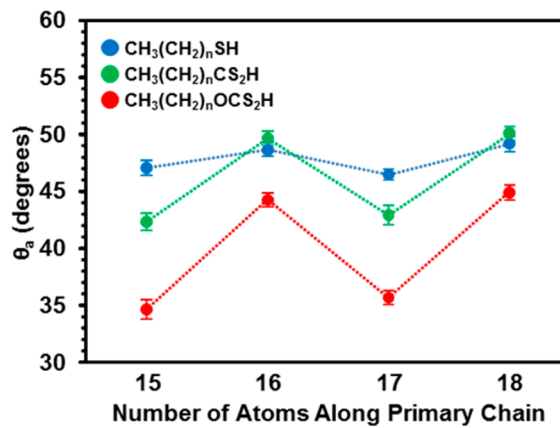


Figure 4. Advancing contact angles of hexadecane on SAMs generated from *n*-alkanethiols, dithiocarboxylic acids, and *n*-alkyl xanthic acids. The *x*-axis represents the total number of atoms in the chain's backbone, a number that is not necessarily equal to *n*. Error bars indicate the standard deviation for the data.

normal.^{35,52} However, an alternative explanation has also been advanced that focuses on the density of atomic contacts made between the SAM interface and the contacting liquid; the greater the interfacial contact area, the greater the van der Waals interactions between the two interfaces.³⁶ No matter which of these phenomena yields the experimental results, the observation of this type of parity effect generally signifies that the underlying gold is of high quality, with relatively large flat domains that promote consistent ordering of the adsorbates along specific orientations.⁵³ As discussed earlier, Colorado et al. observed considerably larger parity effects for ADTCA SAMs in comparison to *n*-alkanethiolate SAMs. We observed a similar trend here, where $\Delta\theta$ ($\theta_a^{\text{even}} - \theta_a^{\text{odd}}$) is approximately 9° for the odd vs even contact angles of hexadecane on both ADTCA and *n*-alkyl xanthate SAMs. However, the measured values of θ_a^{HD} for the *n*-alkyl xanthate SAMs were approximately 6° lower than those measured on their ADTCA equivalents. Consequently, these data suggest that the *n*-alkyl xanthate SAMs share a similar structure with the ADTCA SAMs on the gold surface, but the greater wettabilities of the *n*-alkyl xanthates might indicate that they are somewhat conformationally disordered relative to the ADTCA SAMs.

Characterization by PM-IRRAS. Polarization modulation infrared reflection absorption spectroscopy is an important tool used to probe the terminal group orientations (with respect to the surface normal) and the chain conformations (gauche defects) of organic thin films. We obtained spectra of the C–H stretching region of the *n*-alkyl xanthate SAMs using infrared reflection absorption spectroscopy in order to verify that the odd–even effect observed from the advancing hexadecane contact angle data was in fact due to the changing orientation of the terminal methyl groups as the length of the carbon chain was systematically varied. By examining the IR spectra, it is possible to follow the change in the terminal group orientation by observing the relative intensities of the methyl antisymmetric C–H stretch, $\nu_a^{\text{CH}_3}$, at $\sim 2965 \text{ cm}^{-1}$ and the methyl symmetric C–H stretch, $\nu_s^{\text{CH}_3}$, at $\sim 2878 \text{ cm}^{-1}$.⁵⁴ The PM-IRRAS spectra of the series of *n*-alkyl xanthate SAMs are shown in Figure 5. The spectra of SAMs formed from C16OCS₂H and

C14OCS₂H exhibit a $\nu_a^{\text{CH}_3}$ band of lower intensity than the $\nu_s^{\text{CH}_3}$ band, indicative of a structural alignment wherein the net dipole associated with $\nu_s^{\text{CH}_3}$ for the methyl group is oriented more perpendicular to the surface than parallel. In contrast, for the spectra of the SAMs formed from C15OCS₂H and C13OCS₂H, the $\nu_a^{\text{CH}_3}$ band exhibits a considerably higher intensity than the $\nu_s^{\text{CH}_3}$ band, consistent with a structural alignment in which the net dipole associated with $\nu_s^{\text{CH}_3}$ for the methyl group is tilting roughly parallel to the surface. Thus, films composed of odd-numbered primary chains are terminated by final C–C bonds that are oriented nearly parallel to the gold surface, which in turn creates a greater exposure of the more wettable methylene units and a greater number of interfacial atomic contacts. These data are consistent with the previous study of the ADTCA SAMs where enhanced wettabilities (lower contact angles) were observed for films having odd-numbered primary chain lengths compared to those having even-numbered primary chain lengths.²⁰

To determine whether the NAXA SAMs possess greater conformational disorder (as indicated by their increased wettabilities and lower film thicknesses), a further examination of the PM-IRRAS spectra is necessary. Previous studies have shown that the position of the antisymmetric methylene C–H stretching ($\nu_a^{\text{CH}_2}$) band in *n*-alkanethiolate SAMs is sensitive to the conformational order of the hydrocarbon backbone.^{2,7,55} Porter et al. determined that highly ordered *n*-alkanethiol-based SAMs on gold composed of methylene chains with at least ten carbon atoms exhibited $\nu_a^{\text{CH}_2}$ peak positions between 2918 and 2919 cm^{-1} , which according to the work of Snyder et al. is indicative of trans-extended crystalline conformations for the array of alkyl chains.^{2,55} Accordingly, blue shifts for these bands to higher wavenumbers are attributable to decreased interchain van der Waals interactions and increased alkyl chain disorder (gauche defects).^{2,7,55} As expected, the greater wettabilities observed on the NAXA SAMs probably arise from an increase in conformational disorder since the peak position of the $\nu_a^{\text{CH}_2}$ band increases by approximately 2 cm^{-1} when compared to those of their *n*-alkanethiol and ADTCA analogues.²¹ Another element of the PM-IRRAS spectra that suggests greater conformational disorder in the NAXA SAMs is the peak width at half-height. As alkyl chains become more disordered, the diversity of alkyl chain conformations distributed throughout the film increases, leading to an increase in the width of the $\nu_a^{\text{CH}_2}$ band. The substitution of an oxygen atom for a methylene unit in the NAXA SAMs produces dipole–dipole interactions between neighboring chains, which can give rise to minor changes in chain alignments within the film, interactions that can plausibly contribute to an increase in the width of the $\nu_a^{\text{CH}_2}$ band. Such band broadening is observed in the $\nu_a^{\text{CH}_2}$ bands of the NAXA SAMs when compared to their *n*-alkanethiolate and ADTCA analogues (see Figure 5 and Figure S1 in the Supporting Information).²¹ This broadening is accompanied by an appreciable decrease in $\nu_a^{\text{CH}_2}$ band intensity, a change that can be partly attributed to the decrease by one in the number of methylene units along the backbone of the NAXA adsorbates.

XPS Characterization. X-ray photoelectron spectroscopy can be used to evaluate the nature of the chemical bond between adsorbate headgroups and the substrate surface.⁵⁶ In the case of SAMs on gold, an analysis of the S_{2p} peak binding energy can determine the existence of incomplete adsorbate attachment and/or the formation of multilayers. In *n*-alkanethiolate SAMs, the $S_{2p_{3/2}}$ photoelectrons of unbound

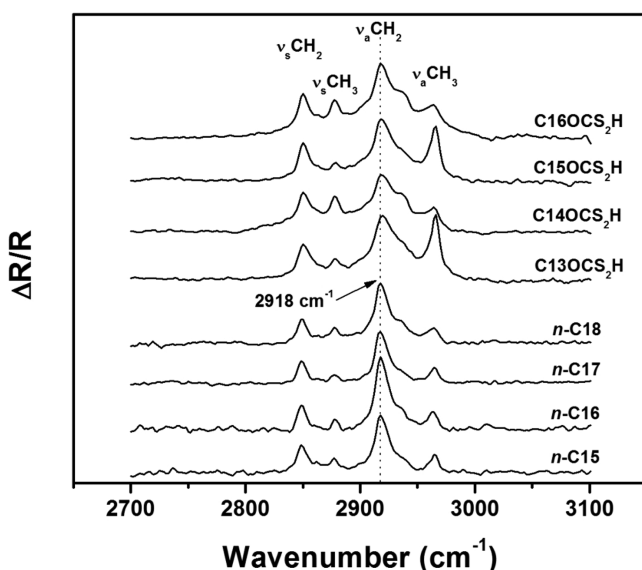


Figure 5. PM-IRRAS spectra of SAMs on gold derived from the series of *n*-alkyl xanthic acids and *n*-alkanethiols.

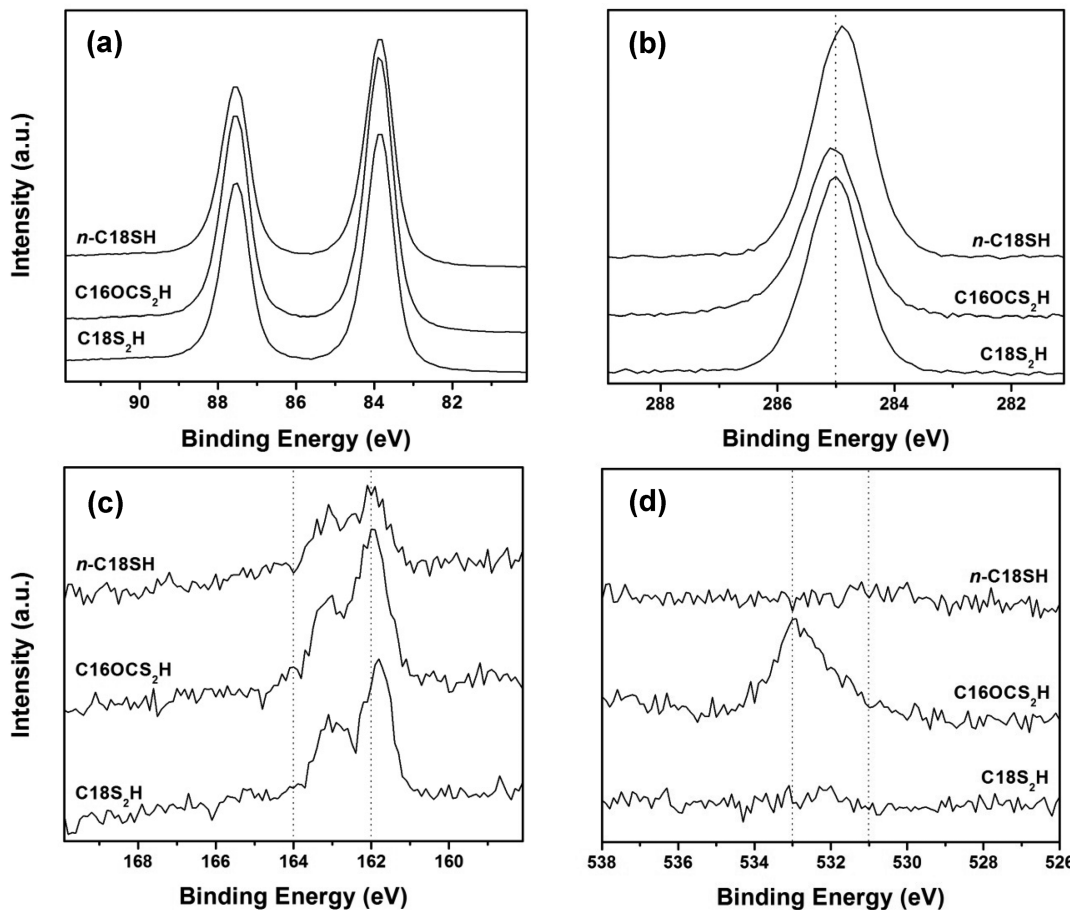


Figure 6. High-resolution X-ray photoelectron spectra of the (a) Au_{4f}, (b) C_{1s}, (c) S_{2p}, and (d) O_{1s} regions for SAMs formed from n-C18SH, C16OCS₂H, and C18S₂H.

thiols display binding energies between \sim 163 and 164 eV, whereas the binding energies of gold-bound thiols appear at \sim 162 eV.⁵⁶ Sulfur species in highly oxidized states exhibit S_{2p_{3/2}} photoelectron binding energies that are greater than \sim 166 eV.⁵⁷ Additionally, XPS is also a useful technique for evaluating the relative atomic composition of self-assembled monolayer films.^{57,58} Specifically, since the experimentally measured intensities of gold depend on the amount (thickness) of the adsorbed carbon overlayer, a comparison of the relative intensities of the XPS spectra binding energies of Au and C can provide information regarding the packing densities of SAMs on gold.⁸

We analyzed the XPS spectra of SAMs generated from our series of NAXAs in the spectral region for the S_{2p} binding energy to determine if the films were solely comprised of gold-bound adsorbates—a result that would indicate the attachment of *both* sulfur atoms in the bidentate headgroup to the surface of gold. A prior study by Ihs et al. of SAMs derived from ethyl xanthate on gold had determined via XPS that these adsorbates bound to the surface equally through both sulfur atoms; however, the alkyl chain was markedly shorter than those examined here.⁴³ Our analysis shows that all of our NAXA monolayers consist of a spin–orbit split doublet with the S_{2p_{3/2}} binding energy at \sim 162 eV, suggesting complete adsorbate binding to the gold surface through both sulfur atoms. Moreover, the absence of peaks \geq 166 eV suggests that no highly oxidized sulfur species were present in any of the films.

Representative XPS spectra of the Au_{4f}, C_{1s}, S_{2p}, and O_{1s} regions of the SAM formed from C16OCS₂H along with its analogues from the ADTCA and n-alkanethiolate series of SAMs are shown in Figure 6.

Estimations of relative adsorbate surface coverages of SAMs by XPS require a calibration of the photoelectron intensities of n-alkanethiolate films having known overlayer thicknesses. This type of quantitative analysis depends on the attenuation of the integrated Au_{4f} peak intensities by the overlaying adsorbate molecules. Since the measured intensities for the binding energies of Au and C depend on the amount of overlying material, adsorbate alkyl chain densities can be estimated by comparing the data collected for the C16OCS₂H film with the standard intensities observed for n-alkanethiolate films having thicknesses and packing densities that are precisely known. An analysis of this sort requires a knowledge of the absolute value of the photoelectron attenuation length, which can be acquired by constructing a calibration curve from the natural logarithm of the observed Au_{4f} intensities versus the number of carbon atoms per adsorbate from a series of SAMs generated from n-alkanethiols of increasing chain length (SAM adsorbates of the form H(CH₂)_xS—Au and abbreviated n-Cx; n-C10, n-C12, n-C14, n-C16, and n-C18). The attenuated Au_{4f} signal is described by eq 1:

$$\ln \text{Au}_n = -nd/(\lambda \sin \theta) + \text{constant} \quad (1)$$

where Au_n is the intensity of the Au_{4f} XPS binding energy signal attenuated by an *n* carbon monolayer, *d* is the thickness of the

Table 1. Integrated Photoelectron Intensities (Counts), Relative Chain Densities, and C_{1s}/Au_{4f} and S_{2p}/Au_{4f} Ratios of SAMs from the Indicated Adsorbates

adsorbate	C_{1s} (counts)	S_{2p} (counts)	Au_{4f} (counts)	O_{1s} (counts)	chain density from Au_{4f} (%)	C_{1s}/Au_{4f}	S_{2p}/Au_{4f}
<i>n</i> -C18SH	22 213	1352	149 358	101	100	0.149	0.009
C18S ₂ H	21 142	2965	153 904	132	99	0.143	0.019
C16OCS ₂ H	16 800	2676	177 012	2251	94	0.095	0.015

SAM per methylene unit, λ is the attenuation length, and θ is the photoelectron takeoff angle. For these calculations, we assumed that the attenuation by sulfur was equivalent to 1.5 carbon atoms per adsorbate. A least-squares analysis of the Au_{4f} signals attenuated by the overlying *n*-alkanethiolates yielded an attenuation length of 41 Å, in close agreement with the value obtained by Bain et al.⁵⁸ We then derived an “effective” number of carbon atoms per adsorbate from the calibration curve and the measured attenuated gold signal from the C16OCS₂H SAM. With these data, we compared the “effective” number of carbon atoms per adsorbate with the actual stoichiometric number of carbon atoms per adsorbate in the C16OCS₂H SAM. We treated the oxygen atom in each C16OCS₂H adsorbate as a methylene unit and, in doing so, assumed that the attenuation difference between oxygen and carbon atoms was negligible for a single atom substitution. This analysis gave an alkyl chain density of approximately 94% for the C16OCS₂H SAM relative to the normalized, densely packed *n*-alkanethiolate SAMs, as shown in Table 1.

Table 1 also shows the integrated peak intensities obtained from the XPS spectra in Figure 6. An examination of the C_{1s}/Au_{4f} and S_{2p}/Au_{4f} intensity ratios can provide additional information regarding the relative adsorbate coverages and relative densities of sulfur. The density of carbon on gold in the C16OCS₂H SAM is noticeably lower than both the C18S₂H and *n*-C18SH SAMs, which were essentially equivalent. The lower C_{1s}/Au_{4f} ratio for the C16OCS₂H SAM can be rationalized on the basis that (1) the C16OCS₂H SAM is composed of adsorbates having one fewer carbon atom per molecule than the other two SAMs and (2) there are fewer molecules per surface area in the C16OCS₂H SAM as indicated by its diminished packing density (vide supra). Notably, the relative importance of stoichiometry (i.e., the first factor) depends partly on whether the attenuation by an oxygen atom is comparable to that of a methylene group.

The S_{2p}/Au_{4f} intensity ratio of the C18S₂H SAM (0.019) was approximately 2 times that of the *n*-C18SH SAM (0.009), which is consistent with a structure that possesses two sulfur atoms per molecule (see Table 1). We anticipated an identical result when examining the S_{2p}/Au_{4f} intensity ratio of the C16OCS₂H SAM (0.015); however, the ratio obtained is consistent with the diminished packing density observed for the NAXA SAM.

Film Stability as a Function of Time and Exposure to Atmospheric Conditions. In the study by Lee et al.,²¹ ADTCA SAMs were examined after exposure to oxygen- and argon-rich environments and ambient laboratory conditions over a period of 2 weeks to determine their relative stability as a function of chain length. In the present study, we evaluate the relative stability of SAMs generated from two *n*-alkyl xanthic acids (C16OCS₂H, C10OCS₂H), two dithiocarboxylic acids (C18S₂H, C12S₂H), and one *n*-alkanethiol (*n*-C18SH) using data collected during ex situ monitoring of the SAMs to determine the nature and amount of organic material that remained on the surface after exposure to various stimuli. To

examine the effect of the atmosphere on SAM degradation, the stabilities of the SAMs were evaluated under various atmospheric conditions (argon, air, and oxygen). SAM-coated wafers were placed in glass vials, sealed with a septum, and purged with the contacting gases for at least 5 min. The vials were then placed in a foil-lined box and directly exposed to a 60 W soft white light bulb. The laboratory temperature was maintained at 23 ± 1 °C, and the temperature directly under the light source was 25 ± 2 °C. After exposure to the various environments for selected time periods, the SAM-coated wafers were thoroughly rinsed with absolute ethanol and dichloromethane and then dried with a stream of ultrapure nitrogen gas before analyzing the films.

Initial ellipsometric thickness measurements were recorded to estimate the film quality prior to exposure to external stimuli. After exposure to various conditions, ellipsometric measurements were collected at 24 h intervals for 4 days to monitor the loss of film thickness as a function of time. In one set of experiments, we exposed the five SAMs to soft white light and an atmosphere of air; these experiments led to the stability profiles in Figure 7. The profiles demonstrate that the initial

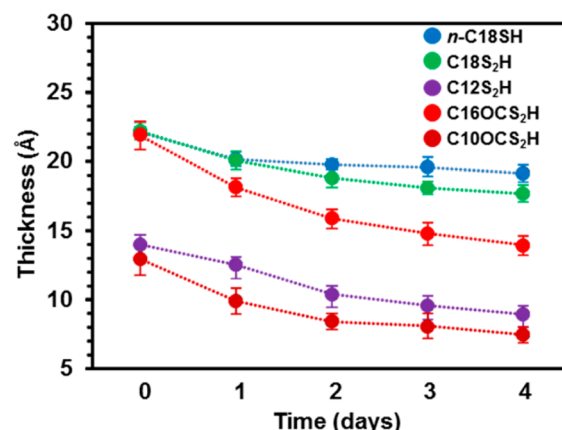


Figure 7. Ellipsometric thickness measurements of various SAMs as a function of time recorded during a stability experiment where the SAMs were exposed to air and soft white light. Error bars indicate the standard deviation for the data.

ellipsometric thicknesses of *n*-C18SH, C18S₂H, and C12S₂H agree well with previous reports and are consistent with the formation of densely packed monolayer films.^{20,21} Furthermore, the data show that the ADTCA and NAXA SAMs undergo significant desorption over a period of only 4 days, where the NAXA SAMs were the least stable compared to the ADTCA and *n*-alkanethiolate SAMs. The data also indicate that films composed of shorter adsorbates undergo considerable desorption, while films composed of longer adsorbates are more resistant to desorption. In contrast, SAMs generated from *n*-alkanethiols exhibited insignificant desorption over the 4 day experiment.

To complement the ellipsometric thickness data, we measured the advancing contact angles of hexadecane to monitor the loss of conformational order over the course of the 4 day exposure to air and soft white light. Figure 8 shows a

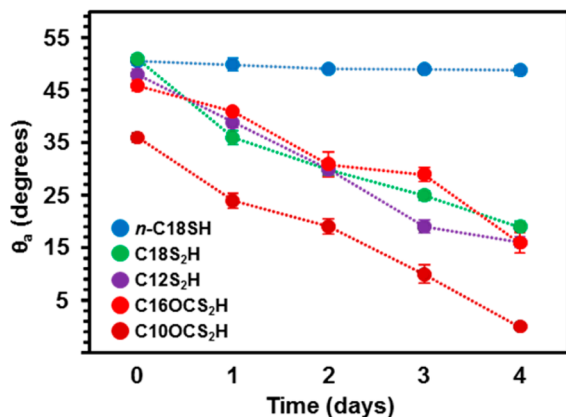


Figure 8. Advancing hexadecane contact angle measurements on various SAMs as a function of time recorded during a stability experiment where the SAMs were exposed to air and soft white light. Error bars indicate the standard deviation for the data.

systematic decrease in θ_a^{HD} over time for all of the SAMs in this experiment. The fastest decrease occurred in the NAXA SAMs having the shortest chain length (i.e., the C10OCS₂H SAM), where hexadecane completely wetted the surface by the fourth day. As a whole, the contact angle data suggest that the NAXA SAMs were more readily susceptible to decomposition under ambient conditions.

In separate studies, we examined the stability of the aforementioned SAMs under oxygen-rich and argon-rich atmospheres. Previous studies have shown that oxygen, or more likely oxygen in the form of atmospheric ozone, readily leads to the decomposition of *n*-alkanethiolate SAMs on gold.^{59,60} Therefore, we subjected the SAMs to an atmosphere known to enhance degradation and compared the resulting data to those collected for SAMs under an inert atmosphere. Figure 9 shows that all of the SAMs exposed to oxygen undergo substantially more degradation than the SAMs exposed to argon. Even the *n*-alkanethiolate SAM, which demonstrated modest film loss in air, displayed an appreciable amount of degradation after prolonged exposure to oxygen. In contrast, the degree of decomposition under argon was markedly less. We note, however, that degradation almost certainly occurs when the SAMs are removed from the inert atmosphere and exposed to the ambient laboratory atmosphere during the course of the ellipsometric measurements.

From these studies, we can classify the observed degradations as follows: (1) under oxygen, fastest degradation; (2) in air, intermediate degradation; (3) under argon, slowest degradation. Also, as we had anticipated, the SAMs generated from adsorbates with longer alkyl chains were more resistant to decomposition, and the resistance increased with increasing chain length. Moreover, SAMs generated from NAXAs were the most susceptible to decomposition (i.e., the least stable), which can be attributed, at least in part, to their lower alkyl chain packing density and their lesser conformational order.

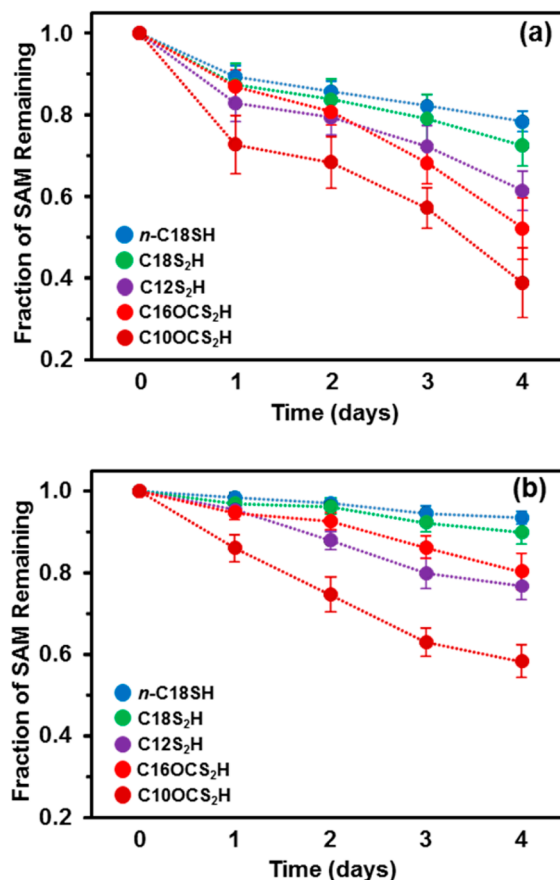


Figure 9. Ellipsometric thickness measurements of various SAMs as a function of time recorded during a stability experiment where the SAMs were exposed to (a) oxygen and (b) argon, both under soft white light. Error bars indicate the standard deviation for the data.

CONCLUSIONS

A series of *n*-alkyl xanthic acids were synthesized to serve as bidentate adsorbates for the generation of SAMs on gold. Optical ellipsometry confirmed that the NAXAs formed monolayers having thicknesses that were similar to those of analogous *n*-alkanethiolate SAMs. The advancing contact angles of water indicated that the NAXA adsorbates generated a predominately methyl-terminated hydrophobic interface. Additionally, the measurements were statistically equivalent across a series of NAXA SAMs of varying adsorbate chain length, indicating (at a primitive level) that the films were compositionally and structurally similar from one adsorbate to the next. The advancing contact angles of hexadecane showed a large “odd–even” effect, consistent with the results obtained for ADTCA SAMs; however, the values of θ_a^{HD} for the NAXA SAMs were ~6° lower on average than those for the ADTCA SAMs. This difference was interpreted to indicate reduced conformational order in the NAXA films. Analysis by PM-IRRAS confirmed that NAXA SAMs were less ordered than analogous ADTCA SAMs based on the relative peak positions of their $\nu_a^{\text{CH}_2}$ bands. Measurements by PM-IRRAS also showed a systematic difference in the terminal group orientation for NAXA SAMs composed of odd- and even-numbered primary chains, providing additional evidence of an odd–even effect for these SAMs. Analysis of the NAXA SAMs by XPS revealed that both sulfur atoms bind to the gold surface and that the packing density for these SAMs was lower than both the *n*-

alkanethiolate and ADTCA SAMs. Stability studies revealed that the NAXA SAMs were more prone to desorption/decomposition than analogous *n*-alkanethiolate and ADTCA SAMs when subjected to a variety of environmental conditions. Overall, these studies revealed the following order of stability: *n*-alkanethiolate SAMs > ADTCA SAMs > NAXA SAMs.

■ ASSOCIATED CONTENT

§ Supporting Information

PM-IRRAS spectra of the SAMs derived from C₁₆OCS₂H, C₁₈S₂H, and *n*-C₁₈SH along with the ¹H and ¹³C NMR spectra for the *n*-alkyl xanthic acids. This material is available free of charge via the Internet at <http://pubs.acs.org>.

■ AUTHOR INFORMATION

Corresponding Author

*E-mail: henry.moore@utb.edu (H.J.M.); trlee@uh.edu (T.R.L.).

Notes

The authors declare no competing financial interest.

■ ACKNOWLEDGMENTS

We are grateful for support from the Robert A. Welch Foundation (Grant No. E-1320), the National Science Foundation (DMR-0906727), and the Texas Center for Superconductivity at the University of Houston. Support for work at the University of Texas at Brownsville was generously provided by a Departmental Grant from the Robert A. Welch Foundation (Grant No. BQ-0038).

■ REFERENCES

- (1) Nuzzo, R. G.; Fusco, F. A.; Allara, D. L. Spontaneously Organized Molecular Assemblies. 3. Preparation and Properties of Solution Adsorbed Monolayers of Organic Disulfides on Gold Surfaces. *J. Am. Chem. Soc.* **1987**, *109*, 2358–2368.
- (2) Porter, M. D.; Bright, T. B.; Allara, D. L.; Chidsey, C. E. D. Spontaneously Organized Molecular Assemblies. 4. Structural Characterization of *n*-Alkyl Thiol Monolayers on Gold by Optical Ellipsometry, Infrared Spectroscopy, and Electrochemistry. *J. Am. Chem. Soc.* **1987**, *109*, 3559–3568.
- (3) Strong, L.; Whitesides, G. M. Structures of Self-Assembled Monolayer Films of Organosulfur Compounds Adsorbed on Gold Single Crystals: Electron Diffraction Studies. *Langmuir* **1988**, *4*, 546–558.
- (4) Ulman, A.; Eilers, J. E.; Tillman, N. Packing and Molecular Orientation of Alkanethiol Monolayers on Gold Surfaces. *Langmuir* **1989**, *5*, 1147–1152.
- (5) Bain, C. D.; Whitesides, G. M. Modeling Organic Surfaces with Self-Assembled Monolayers. *Angew. Chem.* **1989**, *101*, 522–528.
- (6) Dubois, L. H.; Nuzzo, R. G. Synthesis, Structure, and Properties of Model Organic Surfaces. *Annu. Rev. Phys. Chem.* **1992**, *43*, 437–463.
- (7) Ulman, A. *An Introduction to Ultrathin Organic Films*; Academic: San Diego, 1991.
- (8) Park, J.-S.; Vo, A. N.; Barriet, D.; Shon, Y.-S.; Lee, T. R. Systematic Control of the Packing Density of Self-Assembled Monolayers Using Bidentate and Tridentate Chelating Alkanethiols. *Langmuir* **2005**, *21*, 2902–2911.
- (9) Garg, N.; Lee, T. R. Self-Assembled Monolayers Based on Chelating Aromatic Dithiols on Gold. *Langmuir* **1998**, *14*, 3815–3819.
- (10) Shon, Y.-S.; Lee, T. R. Chelating Self-Assembled Monolayers on Gold Generated from Spiroalkanedithiols. *Langmuir* **1999**, *15*, 1136–1140.
- (11) Lim, J. K.; Kim, Y.; Kwon, O.; Joo, S.-W. Adsorption of 1,3-Benzenedithiol and 1,3-Benzenedimethanethiol on Gold Surfaces. *ChemPhysChem* **2008**, *9*, 1781–1787.
- (12) Lee, Y. J.; Jeon, I. C.; Paik, W.-k.; Kim, K. Self-Assembly of 1,2-Benzeneedithiol on Gold and Silver: Fourier Transform Infrared Spectroscopy and Quartz Crystal Microbalance Study. *Langmuir* **1996**, *12*, 5830–5837.
- (13) Bruno, G.; Babudri, F.; Operamolla, A.; Bianco, G. V.; Losurdo, M.; Giangregorio, M. M.; Hassan, O. O.; Mavelli, F.; Farinola, G. M.; Capezzutto, P.; Naso, F. Tailoring Density and Optical and Thermal Behavior of Gold Surfaces and Nanoparticles Exploiting Aromatic Dithiols. *Langmuir* **2010**, *26*, 8430–8440.
- (14) Kim, C. H.; Han, S. W.; Ha, T. H.; Kim, K. o-Xylene- α,α' -dithiol Monolayer Film on Gold: Fourier Transform Infrared Spectroscopy, Quartz Crystal Microbalance, and Atomic Force Microscopy Study. *Langmuir* **1999**, *15*, 8399–8404.
- (15) Singhana, B.; Rittikulsittichai, S.; Lee, T. R. Tridentate Adsorbates with Cyclohexyl Headgroups Assembled on Gold. *Langmuir* **2013**, *29*, 561–569.
- (16) Whitesell, J. K.; Chang, H. K. Directionally Aligned Helical Peptides on Surfaces. *Science* **1993**, *261*, 73–76.
- (17) Kitagawa, T.; Idomoto, Y.; Matsubara, H.; Hobara, D.; Kakiuchi, T.; Okazaki, T.; Komatsu, K. Rigid Molecular Tripod with an Adamantane Framework and Thiol Legs. Synthesis and Observation of an Ordered Monolayer on Au(111). *J. Org. Chem.* **2006**, *71*, 1362–1369.
- (18) Katano, S.; Kim, Y.; Matsubara, H.; Kitagawa, T.; Kawai, M. Hierarchical Chiral Framework Based on a Rigid Adamantane Tripod on Au(111). *J. Am. Chem. Soc.* **2007**, *129*, 2511–2515.
- (19) Fox, M. A.; Whitesell, J. K.; McKerrow, A. J. Fluorescence and Redox Activity of Probes Anchored through an Aminothiol to Polycrystalline Gold. *Langmuir* **1998**, *14*, 816–820.
- (20) Colorado, R., Jr.; Villazana, R. J.; Lee, T. R. Self-Assembled Monolayers on Gold Generated from Aliphatic Dithiocarboxylic Acids. *Langmuir* **1998**, *14*, 6337–6340.
- (21) Lee, T.-C.; Hounihan, D. J.; Colorado, R., Jr.; Park, J.-S.; Lee, T. R. Stability of Aliphatic Dithiocarboxylic Acid Self-Assembled Monolayers on Gold. *J. Phys. Chem. B* **2004**, *108*, 2648–2653.
- (22) Lee, T.-C.; Chen, P.-C.; Lai, T.-Y.; Tuntiwechapikul, W.; Kim, J.-H.; Lee, T. R. Aliphatic Dithiocarboxylic Acids: New Adsorbates for Soft Lithographic Patterning. *Appl. Surf. Sci.* **2008**, *254*, 7064–7068.
- (23) Morf, P.; Raimondi, F.; Nothofer, H.-G.; Schnyder, B.; Yasuda, A.; Wessels, J. M.; Jung, T. A. Dithiocarbamates: Functional and Versatile Linkers for the Formation of Self-Assembled Monolayers. *Langmuir* **2006**, *22*, 658–663.
- (24) Weinstein, R. D.; Richards, J.; Thai, S. D.; Omiatek, D. M.; Bessel, C. A.; Faulkner, C. J.; Othman, S.; Jennings, G. K. Characterization of Self-Assembled Monolayers from Lithium Dialkyldithiocarbamate Salts. *Langmuir* **2007**, *23*, 2887–2891.
- (25) Morf, P.; Ballav, N.; Putero, M.; von, W. F.; Wessels, J. M.; Jung, T. A. Supramolecular Structures and Chirality in Dithiocarbamate Self-Assembled Monolayers on Au(111). *J. Phys. Chem. Lett.* **2010**, *1*, 813–816.
- (26) Miller, M. S.; San, J. R. R.; Ferrato, M.-A.; Carmichael, T. B. New Dialkyldithiophosphinic Acid Self-Assembled Monolayers (SAMs): Influence of Gold Substrate Morphology on Adsorbate Binding and SAM Structure. *Langmuir* **2011**, *27*, 10019–10026.
- (27) San, J. R. R.; Miller, M. S.; Ferrato, M.-A.; Carmichael, T. B. Influence of Alkyl Chain Length on the Structure of Dialkyldithiophosphinic Acid Self-Assembled Monolayers on Gold. *Langmuir* **2012**, *28*, 13253–13260.
- (28) San, J. R. R.; Carmichael, T. B. Formation of Self-Assembled Monolayers with Homogeneously Mixed, Loosely Packed Alkyl Groups Using Unsymmetrical Dialkyldithiophosphinic Acids. *Langmuir* **2012**, *28*, 17701–17708.
- (29) Torrelles, X.; Vericat, C.; Vela, M. E.; Fonticelli, M. H.; Daza Millone, M. A.; Felici, R.; Lee, T.-L.; Zegenhagen, J.; Munoz, G.; Martin-Gago, J. A.; Salvarezza, R. C. Two-Site Adsorption Model for the ($\sqrt{3} \times \sqrt{3}$)-R30° Dodecanethiolate Lattice on Au(111) Surfaces. *J. Phys. Chem. B* **2006**, *110*, 5586–5594.
- (30) Li, F.; Tang, L.; Zhou, W.; Guo, Q. Resolving the Au-Adatom-Alkanethiolate Bonding Site on Au(111) with Domain Boundary

- Imaging Using High-Resolution Scanning Tunneling Microscopy. *J. Am. Chem. Soc.* **2010**, *132*, 13059–13063.
- (31) This assessment of the nature of the fundamental surface structure of SAMs is based upon literature sources that include scanning tunneling microscopy as a critical component in the evaluation of data obtained via other instrumental means.
- (32) Alves, C. A.; Smith, E. L.; Porter, M. D. Atomic Scale Imaging of Alkanethiolate Monolayers at Gold Surfaces with Atomic Force Microscopy. *J. Am. Chem. Soc.* **1992**, *114*, 1222–1227.
- (33) Li, F.; Tang, L.; Zhou, W.; Guo, Q. Relationship Between the $c(4 \times 2)$ and the $(\sqrt{3} \times \sqrt{3})R30^\circ$ Phases in Alkanethiol Self-Assembled Monolayers on Au(111). *Phys. Chem. Chem. Phys.* **2011**, *13*, 11958–11964.
- (34) Tao, F.; Bernasek, S. L. Understanding Odd-Even Effects in Organic Self-Assembled Monolayers. *Chem. Rev.* **2007**, *107*, 1408–1453.
- (35) Tao, Y. T.; Lee, M. T.; Chang, S. C. Effect of Biphenyl and Naphthyl Groups on the Structure of Self-Assembled Monolayers: Packing, Orientation, and Wetting Properties. *J. Am. Chem. Soc.* **1993**, *115*, 9547–9555.
- (36) Shon, Y.-S.; Lee, S.; Colorado, R., Jr.; Perry, S. S.; Lee, T. R. Spiroalkanedithiol-Based SAMs Reveal Unique Insight into the Wettabilities and Frictional Properties of Organic Thin Films. *J. Am. Chem. Soc.* **2000**, *122*, 7556–7563.
- (37) Cimatu, K.; Moore, H. J.; Lee, T. R.; Baldelli, S. Sum Frequency Generation Imaging of Microcontact-Printed Monolayers Derived from Aliphatic Dithiocarboxylic Acids: Contrast Based on Terminal-Group Orientation. *J. Phys. Chem. C* **2007**, *111*, 11751–11755.
- (38) Bunton, C. A.; Salame, J. E.; Sepulveda, L. Micellar Effects on the Acid-Catalyzed Decomposition of Monoalkyl Xanthates. *J. Org. Chem.* **1974**, *39*, 3128–3132.
- (39) Efrima, S.; Pradhan, N. Xanthates and Related Compounds as Versatile Agents in Colloid Science. *C. R. Chim.* **2003**, *6*, 1035–1045.
- (40) Tzhayik, O.; Sawant, P.; Efrima, S.; Kovalev, E.; Klug, J. T. Xanthate Capping of Silver, Copper, and Gold Colloids. *Langmuir* **2002**, *18*, 3364–3369.
- (41) Chinwangso, P.; Jamison, A. C.; Lee, T. R. Multidentate Adsorbates for Self-Assembled Monolayer Films. *Acc. Chem. Res.* **2011**, *44*, 511–519.
- (42) Srisombat, L.; Jamison, A. C.; Lee, T. R. Stability: A Key Issue for Self-Assembled Monolayers on Gold as Thin-Film Coatings and Nanoparticle Protectants. *Colloids Surf., A* **2011**, *390*, 1–19.
- (43) Ihs, A.; Uvdal, K.; Liedberg, B. Infrared and Photoelectron Spectroscopic Studies of Ethyl and Octyl Xanthate Ions Adsorbed on Metallic and Sulfidized Gold Surfaces. *Langmuir* **1993**, *9*, 733–739.
- (44) Talonen, P.; Sundholm, G.; Li, W.-H.; Floate, S.; Nichols, R. J. A Combined *in situ* Infrared Spectroscopy and Scanning Tunnelling Microscopy Study of Ethyl Xanthate Adsorption on Au(111). *Phys. Chem. Chem. Phys.* **1999**, *1*, 3661–3666.
- (45) Gothelf, K. V. Self-Assembled Monolayers of Long-Chain Xanthic Acids on Gold Studied by Voltammetry. *J. Electroanal. Chem.* **2000**, *494*, 147–150.
- (46) Li, Z.; Yoon, R.-H. AFM Force Measurements between Gold and Silver Surfaces Treated in Ethyl Xanthate Solutions: Effect of Applied Potentials. *Miner. Eng.* **2012**, *36–38*, 126–131.
- (47) Sawant, P.; Kovalev, E.; Klug, J. T.; Efrima, S. Alkyl Xanthates: New Capping Agents for Metal Colloids. Capping of Platinum Nanoparticles. *Langmuir* **2001**, *17*, 2913–2917.
- (48) Wenzl, I.; Yam, C. M.; Barriet, D.; Lee, T. R. Structure and Wettability of Methoxy-Terminated Self-Assembled Monolayers on Gold. *Langmuir* **2003**, *19*, 10217–10224.
- (49) Jamison, A. C.; Zhang, S.; Zenasni, O.; Schwartz, D. K.; Lee, T. R. Fibrillar Self-Organization of a Line-Active Partially Fluorinated Thiol within Binary Self-Assembled Monolayers. *Langmuir* **2012**, *28*, 16834–16844.
- (50) Bethencourt, M. I.; Srisombat, L.-o.; Chinwangso, P.; Lee, T. R. SAMs on Gold Derived from the Direct Adsorption of Alkanethioacetates Are Inferior to Those Derived from the Direct Adsorption of Alkanethiols. *Langmuir* **2009**, *25*, 1265–1271.
- (51) O'Hagan, D.; Rzepa, H. S. Some Influences of Fluorine in Bioorganic Chemistry. *Chem. Commun.* **1997**, 645–652.
- (52) Tao, Y. T. Structural Comparison of Self-Assembled Monolayers of *n*-Alcanoic Acids on the Surfaces of Silver, Copper, and Aluminum. *J. Am. Chem. Soc.* **1993**, *115*, 4350–4358.
- (53) Colorado, R., Jr.; Lee, T. R. Wettabilities of Self-Assembled Monolayers on Gold Generated from Progressively Fluorinated Alkanethiols. *Langmuir* **2003**, *19*, 3288–3296.
- (54) Nuzzo, R. G.; Dubois, L. H.; Allara, D. L. Fundamental Studies of Microscopic Wetting on Organic Surfaces. 1. Formation and Structural Characterization of a Self-Consistent Series of Polyfunctional Organic Monolayers. *J. Am. Chem. Soc.* **1990**, *112*, 558–569.
- (55) Snyder, R. G.; Hsu, S. L.; Krimm, S. Vibrational Spectra in the Carbon-Hydrogen Stretching Region and the Structure of the Polymethylene Chain. *Spectrochim. Acta, Part A* **1978**, *34A*, 395–406.
- (56) Castner, D. G.; Hinds, K.; Grainger, D. W. X-ray Photoelectron Spectroscopy Sulfur 2p Study of Organic Thiol and Disulfide Binding Interactions with Gold Surfaces. *Langmuir* **1996**, *12*, 5083–5086.
- (57) Hutt, D. A.; Leggett, G. J. Influence of Adsorbate Ordering on Rates of UV Photooxidation of Self-Assembled Monolayers. *J. Phys. Chem.* **1996**, *100*, 6657–6662.
- (58) Bain, C. D.; Whitesides, G. M. Attenuation Lengths of Photoelectrons in Hydrocarbon Films. *J. Phys. Chem.* **1989**, *93*, 1670–1673.
- (59) Schoenfisch, M. H.; Pemberton, J. E. Air Stability of Alkanethiol Self-Assembled Monolayers on Silver and Gold Surfaces. *J. Am. Chem. Soc.* **1998**, *120*, 4502–4513.
- (60) Zhang, Y.; Terrill, R. H.; Tanzer, T. A.; Bohn, P. W. Ozonolysis Is the Primary Cause of UV Photooxidation of Alkanethiolate Monolayers at Low Irradiance. *J. Am. Chem. Soc.* **1998**, *120*, 2654–2655.